NANO EXPRESS

PAPER

Using pulsed mode scanning electron microscopy for cathodoluminescence studies on hybrid perovskite films

Jordi Ferrer Orri[1,2], **Elizabeth M Tennyson**[1], **Gunnar Kusch**[2], **Giorgio Divitini**[2], **Stuart Macpherson**[1], **Rachel A Oliver**[2], **Caterina Ducati**[2] and **Samuel D Stranks**[1,3,*]

[1] Cavendish Laboratory, University of Cambridge, United Kingdom
[2] Department of Materials Science and Metallurgy, University of Cambridge, United Kingdom
[3] Department of Chemical Engineering and Biotechnology, University of Cambridge, United Kingdom
[*] Author to whom any correspondence should be addressed.

E-mail: sds65@cam.ac.uk **and** cd251@cam.ac.uk

Keywords: hybrid perovskite, cathodoluminescence, pulsed mode, beam damage, hyperspectral mapping

Supplementary material for this article is available online

OPEN ACCESS

RECEIVED
31 December 2020

REVISED
15 April 2021

ACCEPTED FOR PUBLICATION
5 May 2021

PUBLISHED
14 May 2021

Abstract

The use of pulsed mode scanning electron microscopy cathodoluminescence (CL) for both hyperspectral mapping and time-resolved measurements is found to be useful for the study of hybrid perovskite films, a class of ionic semiconductors that have been shown to be beam sensitive. A range of acquisition parameters is analysed, including beam current and beam mode (either continuous or pulsed operation), and their effect on the CL emission is discussed. Under optimized acquisition conditions, using a pulsed electron beam, the heterogeneity of the emission properties of hybrid perovskite films can be resolved via the acquisition of CL hyperspectral maps. These optimized parameters also enable the acquisition of time-resolved CL of polycrystalline films, showing significantly shorter lived charge carriers dynamics compared to the photoluminescence analogue, hinting at additional electron beam-specimen interactions to be further investigated. This work represents a promising step to investigate hybrid perovskite semiconductors at the nanoscale with CL.

1. Introduction

Halide perovskites have emerged as exceptional candidates for next-generation optoelectronic applications, as they are high-performing photoactive materials produced at lower costs and processed in a wider range of conditions than many other traditional semiconductors [1]. Hybrid perovskite thin films are heterogeneous at the micro- and nano- length scales in their optoelectronic, structural and chemical properties [2]. Characterization techniques which reveal the structure-property relations are thus fundamental to understand this family of new materials.

Cathodoluminescence (CL) is a promising candidate for the investigation of emerging semiconductor materials [3]. In this technique, an electron beam excites a semiconductor causing emission of photons, which are subsequently collected and analysed. This allows the optoelectronic properties of the material to be probed at a high spatial resolution.

Guthrey and Moseley [4] recently reviewed the body of work on how CL has been helpful to understand these novel halide perovskite materials. Here, we focus on CL signals from scanning electron microscopy (SEM). SEM-CL can produce sub-micrometer spatially resolved maps of optoelectronic emission properties, which can be related to phase composition, defects, impurities and degradation products, both in top-view and cross-section geometries [4]. Numerous studies discuss how the focused high-energy electron beam interacts with the specimen causing reversible and irreversible changes, in a process generally known as beam damage. Methylammonium lead iodide films ($MAPbI_3$), the most widely studied hybrid perovskite structure, and subsequent hybrid perovskite compositions, are highly sensitive to the current and energy of the electron beam. These can result in knock-on damage, inelastic scattering and localized heating, which can promote the loss of

the more volatile (organic) species [5–7]. These phenomena are correlated with a decrease in CL intensity of the perovskite peak and with the emergence of additional emission peaks [8, 9]. For $MAPbI_3$ the emergence of PbI_2 is observed upon degradation, whereas for formamidinium (FA) containing compositions other degradation pathways involving Pb^0 formation and the loss of an iodide molecule are reported [10]. Some electron beam irradiation effects resemble modifications observed under light exposure, [6] ascribed to similar transient changes such as iodide segregation leading to peak broadening and shifts [11]. While the electron beam interaction could be used as an accelerated platform to understand the material stability, electron beam damage is generally undesired for CL analysis. Some general guidelines exist to reduce beam damage, mainly by reducing the beam current and acquisition time, and optimising the acceleration voltage and specimen temperature [4].

CL has been used to characterize semiconductors at the nanoscale for many decades [3]. However, only recent innovations have allowed this technique to move beyond the well-established continuous wave (CW) electron beam CL imaging. Since the creation and application of an optically driven pulsed mode (PM) electron gun adapted to acquire CL, [12] it is now possible to measure time-resolved cathodoluminescence (TRCL) using bright picosecond pulsed electron beams. Such systems enable the probing of picosecond charge-carrier dynamics at the nanoscale, as has been extensively done for III-V semiconductor nanostructures, overcoming some of the limitations of older beam-blanking based PM techniques [13]. For hybrid halide perovskites, Cortecchia *et al* [14] showcased the possibility of using such a system to probe the dynamics of 2D/3D perovskite nanocrystals. They identified heterogeneity of the self-assembled phases of different dimensionality, and probed the TRCL recombination dynamics for each phase, exhibiting both Auger ultrafast recombination in the range of picoseconds and slower TRCL traces matching the time-resolved photoluminescence dynamics. Zhao and Lian *et al* [15] used such a system to study the improvements in luminescence efficiency, uniformity, and lifetime of mixed-dimensional perovskite films after layer and additive engineering.

In addition to enabling the acquisition of TRCL, the use of a pulsed beam can reduce the beam current to tens to hundreds of pA [16]. Low-injection conditions can be tuned to match *operando* conditions of optoelectronic devices, making this technique interesting from a device characterization perspective. More importantly, low-current pulsed beams allow the material to relax electronically and thermally in between pulses, which can be beneficial to hinder beam damage [17, 18]. While the vast majority of historical CL work has been performed on traditional inorganic semiconductors, which show little to no beam damage, the use of a PM electron beam for CL acquisition on hybrid perovskite materials is of interest.

This work aims at comparing CL in the SEM from a CW and PM electron beam for the characterization of thin films of a well studied hybrid perovskite composition, namely the triple-cation double-halide $(FA_{0.79}MA_{0.16}Cs_{0.05})Pb(I_{0.83}Br_{0.17})_3$. This composition is one of the most stable for optoelectronic applications such as solar cells [19]. We investigate how SEM acquisition parameters, especially beam current and beam mode (wither CW or PM), affect the quality of the CL data for these perovskite thin films on glass substrates.

2. Methods

2.1. Fabrication of the hybrid polycrystalline perovskite film

Glass coverslips (18 mm × 18 mm, 0.13–0.17 mm thickness, Academy) were cleaned in acetone and isopropanol (10 min each) in an ultrasonic bath. The substrates were treated for 10 min in an oxygen plasma cleaner immediately before the spin-coating procedure.

The perovskite precursors solutions were prepared by first dissolving PbI_2 (1.1 M), $PbBr_2$ (0.22 M), FAI (1.0 M) and MABr (0.2 M) in a mixture of anhydrous DMF and DMSO (4:1 v:v). CsI solution (1.5 M in DMSO) was then added to the precursor solution as 5% of the total volume. To form the $(FA_{0.79}MA_{0.16}Cs_{0.05})Pb(I_{0.83}Br_{0.17})_3$ thin films, 50 μl of precursor solution was deposited on each substrate. A two-step spin-coating procedure was used for the thin film formation: 10 s at 1000 rpm, 20 s at 6000 rpm. Chlorobenzene (120 μl) was deposited onto the spinning substrate 10 s before the end of the procedure. Films were annealed at 100 °C for 1 h. Lead halide precursors were supplied by TCI, organic compounds were supplied by Greatcell Solar, CsI and solvents were supplied by Sigma.

The film was fabricated at a small fraction of PbI_2 excess, as it is known to suppress non-radiative recombination for mixed halide mixed cation compositions [19, 20]. The sample had been exposed to ambient laboratory air for previous characterization measurements for ~10 h, and was consistently contained within a nitrogen box between measurements. The CL and PL emission was checked to match the PL emission reported for similar compositions prior to the experiment.

2.2. CL hyperspectral mapping and TRCL

A series of 30 CL hyperspectral maps (CL maps) were acquired at different regions on the perovskite film. CL mapping was performed in an Attolight Allalin 4027 Chronos CL-SEM. The spectra were acquired with an iHR320 spectrometer (focal length of 320 mm, 150 gratings per mm blazed at 500 nm, 700 μm entrance slit)

and an Andor 1024 pixel charge-coupled device (readout rate of 3 MHz, horizontal binning of 2 and ×2 signal amplification). All the measurements were performed at room temperature under high vacuum ($<10^{-7}$ mbar). Beam focusing before each CL map was performed on regions of the sample at least 100 μm away from those used for the measurements.

CL maps were taken at various acquisition conditions, as described in table S1 (available online at stacks.iop.org/NANOX/2/024002/mmedia) in the supporting information (SI). These maps were taken at 3 or 6 kV acceleration voltage, at various dwell times from 22 to 502 ms, and at different rastering pixel sizes ranging from 25 to 250 nm. The CL interaction depth at 3 and 6 keV is estimated to be ∼100 and ∼250 nm, respectively, as calculated in the figure S8 in the SI. The electron beam current was modified from 62.5 pA to 10 nA in continuous-wave (CW) beam mode, or from 14 to 115 pA in pulsed mode (PM). PM was obtained by pulsing an electron gun with the third harmonic of an Nd:YAG laser (355 nm) at a pulse width of 7 ps and a frequency of 80.6 MHz (12.41 ns). All beam currents were calibrated using a Faraday cup.

Time-resolved CL measurements were recorded with a time-correlated single photon counting photodetector at an acceleration voltage of 6 kV and beam current of 115 pA. The resolution of the photodetector is 80 ps. Dwell times were extended until the TRCL signal was two orders of magnitude higher than the background, which varied from 60 to 400 s for each peak of interest.

2.3. Processing of the CL data

CL maps were analysed in LumiSpy 0.1 (a Hyperspy-based open-source Python library for luminescence data analysis) [21]. All spectra were background subtracted, cosmic-rays saturating the spectrometer were removed, and the edges of each map were cropped, as these tend to show higher CL intensities due to uneven beam dwelling at the corners as well as edge effects.

Fitting of the data enables the extraction of the emission shape parameters of the CL signal. Three Gaussian distributions and a constant background offset were used to fit CL data, following:

$$\begin{aligned} y(x) &= k_{bkg} + g_{Pvk}(x) + g_{intermediate}(x) + g_{PbI_2}(x) \\ \text{with } g_i(x) &= I_{CL,i} \exp\left\{-4\frac{\log(2)(x - x_{0,i})^2}{FWHM_i^2}\right\} \end{aligned} \tag{1}$$

where each Gaussian represents one of the three peaks of interest in this work (the perovskite, the intermediate degradation phase and the PbI_2 peaks). Each Gaussian is described by x_0: the central peak position, I_{CL}: the peak height at the central position and *FWHM*: the full-width half-maximum of the peak.

Equation (1) was fitted to the spatially averaged CL spectra for each map acquired to generate figure 1. Similarly, the Gaussians were fitted to the CL maps, resulting in spatially-resolved fitted hyperspectral maps, as shown in figure 2.

TRCL decays were normalized and smoothed using a 10-point mean filter before the 1/e values were found.

3. Results and discussion

A systematic study of how acquisition parameters, especially beam mode and beam current, affect the CL maps of hybrid perovskite films is discussed. Under optimized conditions the perovskite phase exhibits the most robust emission features, which we consider evidence for a more pristine crystal structure.

3.1. Optimization of the conditions for CL studies on hybrid perovskite films

A series of 30 CL maps were taken at different positions of a hybrid perovskite film under various acquisition conditions. For each map, the spatially averaged CL spectrum was reported. Figure 1 shows how the mean emission spectra are affected by various acquisition parameters. Figure 1(a) shows a subset of the mean spectra acquired at beam currents ranging from 14 pA to 10 nA, with darker colours representing higher beam currents; and acquired at two different electron beam modes, continuous line for CW, dashed line for PM. The absolute CL intensity values were normalized by the acquisition dwell time of each scan and all the spectra in figure 1(a) were acquired at the same pixel size of ∼120 nm.

In figure 1(a), three main peaks are observed: the main perovskite peak at 740–760 nm (1.68–1.63 eV), [19] a peak corresponding to PbI_2 at 507–518 nm (2.39–2.45 eV), [22] and a broad intermediate peak ranging between 650 and 740 nm (1.68–1.90 eV). The PbI_2 peak is primarily ascribed to the small fraction of PbI_2 excess during the fabrication of the film [19]. The broad intermediate peak is referred to as the intermediate degradation phase, as it only becomes prominent in conjunction with electron beam illumination (see figure S2 in the SI). For each peak, the quality of the CL signal was determined from the parameterized variables of fitting the Gaussian models on the mean emission spectra for each map. More specifically, the fitted central peak position (x_0) and

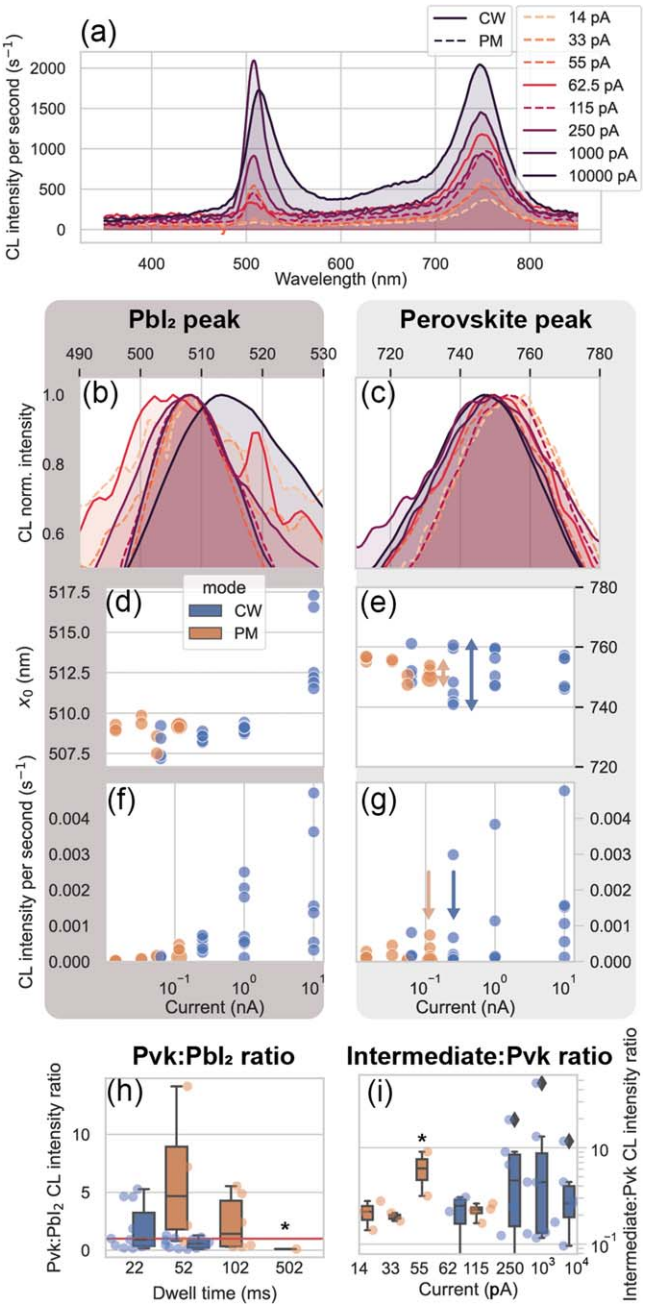

Figure 1. Optimization of the CL acquisition conditions for $(FA_{0.79}MA_{0.16}Cs_{0.05})Pb(I_{0.83}Br_{0.17})_3$ thin films. (a) The spatially averaged CL spectra for a series of CL maps taken at different beam modes (continuous line in CW, dashed line in PM), at different beam currents (darker colours represent higher currents), keeping all other parameters unchanged and the CL intensity normalized to the pixel dwell time. The PbI_2 and the perovskite peaks are visible, as well as an intermediate degradation broad peak. (b), (c) Normalized CL peaks for the (b) PbI_2 and (c) perovskite peaks, with visible peak position shifts. (d)–(i) Correlation of the beam current in nA, the beam mode (CW in blue, PM in orange), and dwell time (from 22 to 502 ms from smaller to larger dots) with respect to different emission peak parameters are shown. (d), (e) The fitted central peak position x_0 of the PbI_2 and the perovskite peak, respectively. (f), (g) The CL intensity (I_{CL}) for the PbI_2 and the perovskite fitted peaks, respectively. (h) The perovskite to PbI_2 CL intensity ratio correlated to pixel dwell time. (i) The intermediate degradation peak to the perovskite CL intensity ratio correlated to beam current. The asterisk (*) shows scans with long dwell times of 502 ms.

peak intensity (I_{CL}) of the different emission peaks were taken as indicators for signal quality. These indicators were then correlated with the respective acquisition parameters at which each CL map was taken, such as beam current, beam mode, acceleration voltage, rastering pixel size, or dwell time, to mention a few. Some parameters were found to have a bigger effect on the CL signal quality than others. These are discussed in depth below.

Figures 1(b)–(i) shows the effect of the electron beam current, beam mode (either CW or PM), and dwell time, on the fitted peaks for each map. The perovskite and PbI_2 emission peaks are analysed separately, as the perovskite peak appears to be more sensitive to electron irradiation, while the PbI_2 peak remains largely unaffected upon continuous electron beam exposure of up to 90 s (see figure S2 in the SI for the evolution of each peak over beam exposure). Figures 1(c) and (e) show that the perovskite peak position x_0 is dependent on the

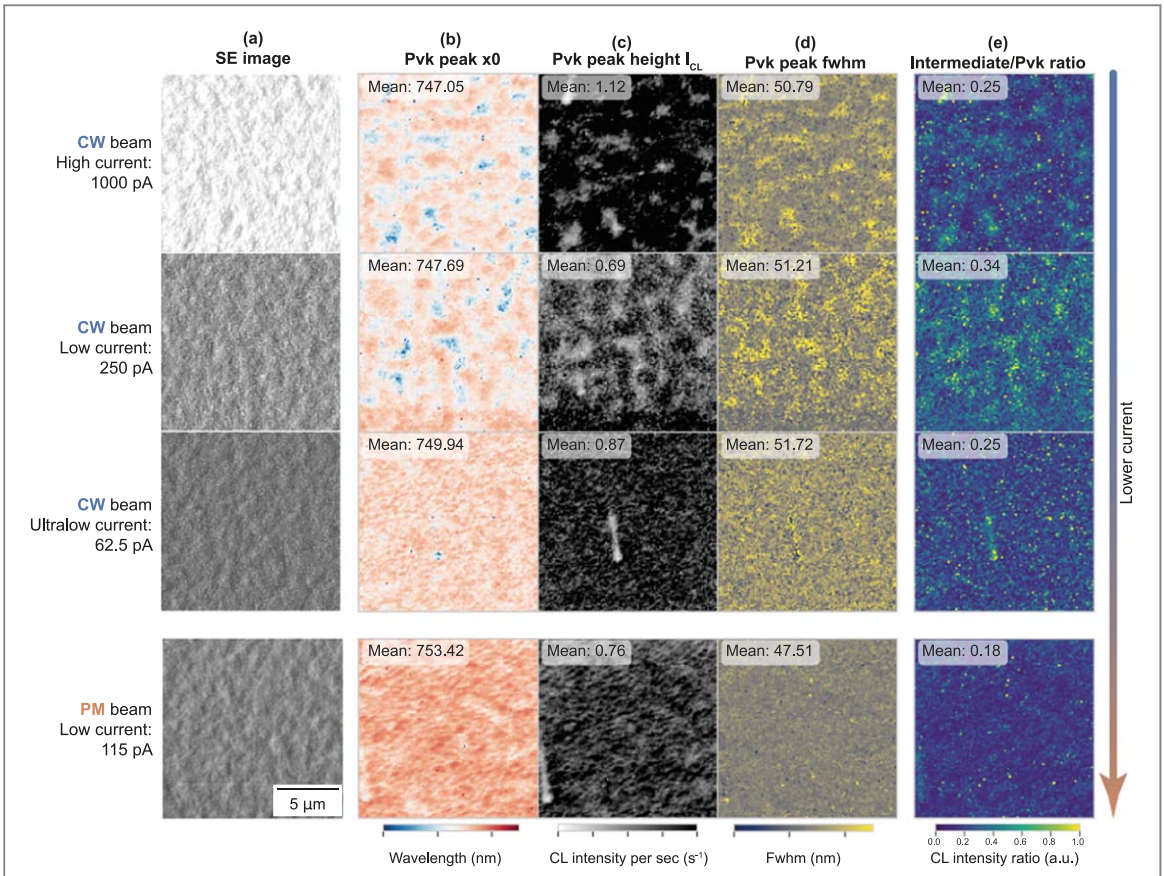

Figure 2. Heterogeneity of CL emission and SEM images of $(FA_{0.79}MA_{0.16}Cs_{0.05})Pb(I_{0.83}Br_{0.17})_3$ thin films under improving acquisition conditions: from suboptimal at the top towards more optimized conditions at the bottom (first three rows are taken in CW mode and the last row in PM). (a) The SEM and (b)–(d) the fitted parameter CL maps for the perovskite peak, with (e) showing the intermediate degradation phase peak to perovskite peak CL intensity ratio, a measure of beam damage. The mean values are reported on the top left for each map.

electron beam current (ranging between 14 pA to 10 nA) and the beam mode (blue for CW and orange for PM). Larger spreads of the values of the perovskite peak positions are observed under CW mode when other parameters such as pixel size or dwell time are changed. For example, marked in figure 1(e), we observe a spread of x_0 of 750 $\pm$ 10 nm (~50 meV) at 250 pA in CW, while at similarly low-current conditions of 115 pA in PM, a spread of x_0 shifts of 750 $\pm$ 3 nm (~10 meV) is measured. At comparable currents we find that PM allows for a more robust CL detection for the perovskite peak.

Figure 1(c) shows a small blue-shift of a few nanometers (~10 meV) between the perovskite peak emission in CW and PM. Blue-shifts at higher currents may be explained by the formation of beam-induced defects and by the Burstein-Moss effect, in which large charge carrier populations can saturate the band edge and populate higher vibrational energy states of the conduction band [8, 11, 14, 23]. At 115 pA and 6 keV, charge carrier concentrations in PM are estimated to reach concentrations as large as $\sim 10^{18}$ $e^- - h^+$-pairs cm^{-3}, assuming a cubic interaction volume of 200 nm depth (see the SI for the estimation). The pulsed nature of the beam would allow carriers to relax, if the time-delay between each electron pulse is larger than the charge-carrier relaxation time, resulting in lower blue-shifts than in CW mode. Figure 2(b), discussed later, is in agreement with this observation of blue-shifts, with spatially averaged perovskite peak emission at 746–749 nm (1.66 eV) in CW compared to 752 nm (1.65 eV) in PM.

Figure 1(g) shows the effect of the perovskite peak intensity (I_{CL}) as a function of beam current and beam mode. For the perovskite peak, we find that PM acquisition can achieve CL intensities as large as those achieved in CW with twice the amount of current (250 pA in CW and 115 pA in PM). However, only low beam currents can be accessed in PM, which strongly limits the intensity of the CL signal.

The analysis of the PbI_2 peak shows different trends, in which most of the observations seen for the beam-sensitive perovskite peak are not applicable. Figures 1(b) and (d) show a narrow spread of the peak position x_0 under both CW and PM, in the range of 3 nm (10 meV), when other parameters such as pixel size or dwell time are changed. A red-shift of the PbI_2 peak from 508–510 nm to 512–517 nm (2.43–2.44 to 2.40–2.42 eV) is observed when the largest beam current of 10 nA is used. This small red shift may be explained by the pre-existing PbI_2 crystallites in the film growing thicker under excessive electron irradiation, as PbI_2 single crystals

show thickness dependent photoluminescence [22]. PbI_2 degradation can also result in the creation of defects and peak shifts, consistent with these observations [24, 25]. For currents of 1 nA and lower, such red shifts are not observed. Hence, PbI_2 is a more stable phase and it is not as susceptible to beam damage as the perovskite phase, as suggested from the evolution of each peak upon beam exposure (figure S2). Figure 1(f) shows the peak intensity increasing proportionally to the current used. The PbI_2 CL emission acquisition does not benefit from using PM in the same way the perovskite phase does.

Given the relative stability of the PbI_2 peak, its intensity can be used as a reference from which to compare the perovskite peak intensity for each acquisition condition. In a pristine specimen, the ratio between the perovskite (Pvk) and the PbI_2 peak intensities (Pvk:PbI_2 ratio) is expected to be larger than 1 as the perovskite peak dominates. The ratio can decrease due to electron beam irradiation, and this can be taken as a measure of beam damage. Figure 1(h) shows that the Pvk:PbI_2 ratio is strongly related to dwell time and to beam mode (also to beam current, as shown in the figure S9 in the SI). At dwell times of 52 ms the Pvk:PbI_2 ratio is one order of magnitude larger for PM than for CW, and this suggests that PM is significantly better at preserving the pristine perovskite phase. However, at extremely low-current conditions, especially in PM, longer dwell times are required to acquire signal-to-noise ratios (SNR) sufficient to discern the background from the signal at each pixel. Longer beam exposures appear to enhance the degradation effect on the perovskite, as seen at larger dwell times of 102 or 502 ms in figure 1(h). A compromise between beam current and dwell time is thus needed to minimize the changes of the perovskite peak.

Another interesting feature is the intermediate degradation phase peak, which can be fitted with a broad Gaussian between 650 and 740 nm (1.68–1.90 eV). A ratio between the Pvk and the intermediate degradation peak intensities can be calculated (intermediate:Pvk ratio) as the former appears as the latter decays. The lower this ratio, the more pristine the perovskite. Figure 1(i) shows how the intermediate:Pvk ratio is affected as the beam current increases and as CW or PM is used. The degradation intermediate phase is more prominent when high beam currents above 1 nA are used in CW mode, as seen from the ratio increasing by one to two orders of magnitude than when lower currents are used. Both for low CW currents of 62.5 and 250 pA and for PM, the degradation peak is low in intensity. Long dwell times in PM are correlated with the appearance of this degradation phase, marked with an asterisk on the figure. Dose, the combination of beam current and dwell time, is thus affecting the appearance of the intermediate degradation phase.

The appearance of higher energy emission features than the perovskite phase is in agreement with other works studying electron beam damage [6, 26, 27]. While the nature of the intermediate degradation phase cannot be conclusively assigned from this CL analysis alone, it can be attributed to a series of factors. The low activation energy of halide-related defects enhances the vulnerability of these materials to beam-induced degradation, [28, 29] which results in a broad distribution of trap states that can be optically active and detectable if present in large densities. Moreover, loss of the more volatile iodine species due to electron beam irradiation could also result in the observed blue shifts. Halide demixing across films has been reported after light soaking or device operation, showing facile halide redistribution between the surface and interface [30–32]. The formation of beam-induced small nanoscale crystallites could also result in a distribution of blue-shifted emission due to confinement effects [33]. Finally, the blue shift could also be attributed to electron beam driven amorphization of the perovskite phase, in agreement with similar high-energy emission peaks observed from pressure-induced amorphization [34].

Other acquisition parameters were found to have a smaller effect on the CL signal quality, such as the field of view, raster scan size, or electron beam energy, which are shown in figures S5–S7 in the SI. The effect of the first two is convolved with the dwell time effect, already discussed. The effect of acceleration voltage is consistent with previous studies, [8, 27, 35–38] in which lower acceleration voltages probe the optical properties at the surface while at higher beam energies the bulk is probed, which can emit differently than the surface. Photons generated deeper in the bulk can also be absorbed by the perovskite layer and not contribute to the collected CL intensity. In general, beam damage is more sensitive to increasing beam current than to acceleration voltage [26].

In short, PM has been found beneficial for the acquisition of CL on triple-cation double-halide hybrid perovskite films, in comparison to CW mode. However, when PM is used, the beam current and dwell time need to be carefully adjusted in order to obtain sufficient SNR while maintaining the perovskite emission. We find that >115 pA and <50 ms, under the experimental conditions and samples reported here, give the best results. Despite the optimization in the acquisition, PM CL still exhibits some secondary features related to beam damage.

3.2. The potential of pulsed mode SEM CL on hybrid perovskite films

We use SEM CL to map the nanoscale heterogeneity of perovskite polycrystalline films. Figure 2 shows a series of CL maps for the fitted perovskite peak taken at different positions on the same perovskite film. The perovskite peak emission changes for spatially resolved CL maps as a function of acquisition conditions. We observe a gradual modification of the perovskite peak quality, measured in terms of the fitted Gaussian position x_0 (figure 2(b)), peak height I_{CL} (figure 2(c)), and peak full-width half-maximum (*FWHM*, figure 2(d)), as a function of beam current. In

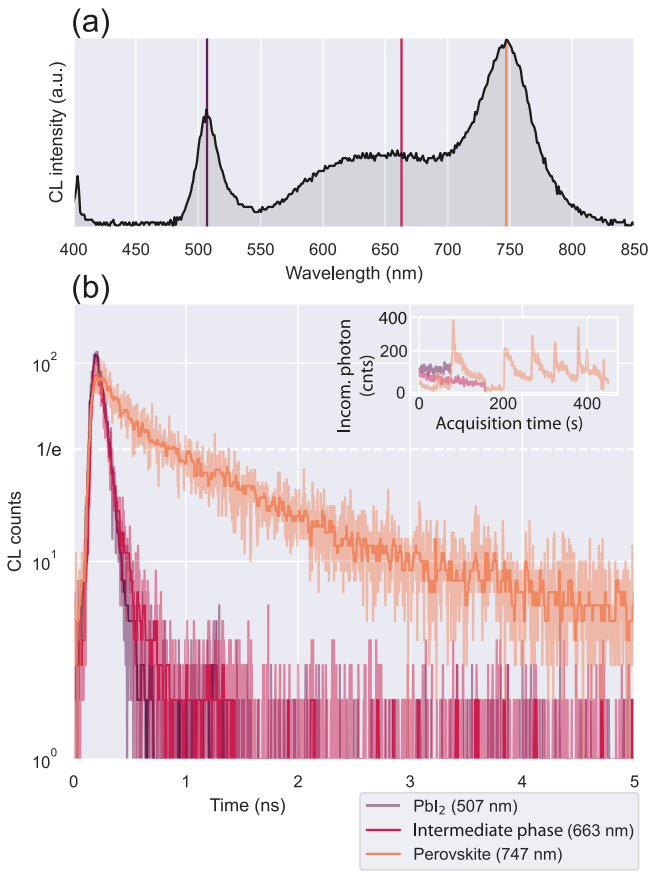

Figure 3. TRCL measurements on a $(FA_{0.79}MA_{0.16}Cs_{0.05})Pb(I_{0.83}Br_{0.17})_3$ perovskite thin film at acceleration voltage of 6 kV and beam current of 115 pA in PM. (a) The CL emission spectrum with the perovskite peak, the PbI_2 peak and a broad intermediate degradation phase. (b) TRCL spectra of the three peaks of interest (smoothed signal as darker line). The inset shows the incoming photon counts per second. The 1/e intensity line is shown on the y-axis.

general, the CL maps acquired at higher currents show more heterogeneous distributions of the perovskite peak features. Figure 2(e) shows a lower intermediate:Pvk intensity ratio for lower beam currents, suggesting a more pristine perovskite emission due to a reduction in beam damage and more homogeneous charge carrier recombination pathways. The least significant beam damage is recorded under PM, at a mean intermediate:Pvk ratio of 0.18 (see figures S12 in the SI for the histograms of the pixel distribution of this ratio). In PM, longer pixel dwell times, twice as long as in CW mode (from 22.28 ms in CW to 52.28 ms in PM), were used. These dwell times were short enough, within the threshold shown in figure 1(h), to result in no increment of beam damage. CL maps acquired in PM at lower currents of 14 or 33 pA resulted in reduced signal quality if dwell times of 52 ms were used, which complicated spectral fitting in a per-pixel basis (figure S11 in the SI).

The switch from CW to a PM electron beam under similar low-current conditions of 62.5 and 250 pA in CW and 115 pA in PM, reveals a further improvement in data acquisition in terms of peak consistency. Figure 2(d) shows a reduction in the *FWHM* magnitude and a more homogeneous distribution for the PM than in CW mode. Similarly, figure 2(b) shows a more homogeneous peak position distribution for PM.

Finally, the use of the optimized PM acquisition conditions enables the study of TRCL decays of the different phases found in the films. Figure 3 shows the acquisition of spatially averaged TRCL decays on a hybrid perovskite polycrystalline film for the first time. Figure 3(a) shows the three peaks of interest selected for the TRCL signal at 507, 663 and 747 nm (2.45, 1.87 and 1.66 eV) for the PbI_2, intermediate degradation phase and perovskite phase, respectively. The PbI_2 and intermediate phases are shorter lived than the perovskite phase, as shown in figure 3(b). The 1/e time decay value for the perovskite peak is found at 0.7 ± 0.1 ns. The lifetimes for the PbI_2 and intermediate phase TRCL decays could not be resolved as they are below the resolution limit of the detector (80 ps). The understanding of the dynamics and nature of these phases are beyond the aims of this work, hence we only present the 1/e value and no fitting models.

Despite the optimization of the experimental conditions used to acquire the TRCL data, the perovskite peak degraded continuously, as shown in the inset in figure 3(b). The inset shows the time evolution of the incoming photon counts to the time-correlated single photon counting photodetector for each peak over continuous beam exposure in PM. For the perovskite peak, the spikes in the photon count correspond to each of the 6

different regions of the sample that were scanned during TRCL acquisition. The perovskite emission completely degraded within 50–100 s of continuous beam rastering (similar to the spectral time evolution shown in figure S2 in the SI). In order to acquire SNR of two orders of magnitude, several different regions were rastered. For the PbI_2 and the degradation higher energy peaks, only a single region was scanned to achieve the desired SNR.

The PbI_2 and the intermediate degradation phase exhibit extremely short-lived dynamics. These short TRCL curves may be attributed to the highly localized formation of these phases, in which charge carriers are produced in a confined volume at high densities, thus affecting lifetimes due to the nature of the bimolecular recombination. For the perovskite peak, the longer-lived carrier dynamics may be attributed to the large grains in the film, which can disperse the charge carriers, formed locally by the electron beam, across the grain. However, these lifetimes are significantly shorter than time-resolved photoluminescence measurements of similar compositions, in the order of hundreds of nanoseconds [39]. These shorter lifetimes may suggest degradation of the perovskite phase by the creation of beam-induced defects, which are visible in the broad intermediate degradation peak and act as charge carrier quenching pathways. Moreover, Auger processes may play a role due to the higher carrier densities produced in CL compared to PL, of the order of $\sim 10^{18}$ $e^- - h^+$-pairs cm^{-3}, [40] which has also been seen in less beam-sensitive materials [41]. Similar perovskite formulations, containing mixed iodide and bromide, are known to show higher Auger rates when the bromide fraction increases due to gradual changes in phase structure, which may here be caused by beam degradation [39].

In short, figures 1 and 2 have shown a more efficient data acquisition of the perovskite emission when a PM electron beam is implemented. Given a CW and a PM electron beam at the same beam current, the PM beam produces short pulses of higher electron currents while the CW produces a constant flux of lower electron currents, both resulting in the same effective current. The higher excitation density in PM can produce larger densities of charge carriers which could saturate non-radiative recombination sites and lead to overall stronger emission. In CW mode, if currents are too low, the non-radiative recombination sites may never be saturated and a smaller fraction of recombination would be radiative. It is therefore the nature of a pulsed beam that could allow for a more efficient CL acquisition (see schematic S13 in the SI). These mechanisms may not be applicable to materials with longer lifetimes, as charge carriers would remain in the excited state for a longer time and the PM would give similar effects as the CW beam. In these cases, the higher efficiency in CL acquisition using PM would not be as pronounced. However, given that electron beam damage may be unavoidable for beam sensitive materials such as hybrid perovskites, the TRCL lifetimes are likely to be shorter than those measured with optical excitations of the pristine structure, in favour of PM.

3.3. Outlook

We have shown the benefits of using a PM electron beam on hybrid perovskite films. It unlocks the use of SEM CL on beam-sensitive hybrid perovskite materials and enables the acquisition of hyperspectral maps with high spatial resolution. CL can thus be used to explore the heterogeneity of optical properties at the nanoscale, at smaller length scales than photoluminescence. TRCL, enabled by the use of a PM electron beam, can be useful to understand the carrier dynamics of these materials at high excitation densities, especially interesting for light emission devices.

CL on beam-sensitive materials is affected by beam damage, and hence must be acquired under scrupulous management of the acquisition parameters. After optimization of the acquisition conditions, CL still exhibits features related to the beam damage; unambiguously assigning the nature of these degradation features in the scanned regions of interest will be the subject of future work. In this work we have analysed mainly the effect of beam current, dwell time and beam mode, yet other parameters should be further investigated. For example, it was shown that temperatures as low as 80 K can hinder the formation of intermediate degradation high-energy peaks in mono-cation mono-halide perovskite compositions [8]. The modification of the pulse rate in PM electron beams may also further improve the CL acquisition for beam sensitive materials, as longer separations between the pulses may allow the beam sensitive material to fully relax electronically and thermally. Finally, further work on sample stabilization may result in beam damage mitigation. For example, the addition of contact layers or the characterization of devices instead of films may help dissipate charges and prevent volatile species from leaving the sample [42]. Such approaches will be the subject of future work.

4. Conclusion

We have systematically studied the parameters affecting the acquisition of CL maps of hybrid perovskite $(FA_{0.79}MA_{0.16}Cs_{0.05})Pb(I_{0.83}Br_{0.17})_3$ films on glass, such as the effect of beam current, dwell time or beam mode. PM electron beams have been found to be useful for the study of triple-cation double-halide perovskite films, yielding more robust results than CW mode. Using PM, the CL spectra strongly resembles pristine perovskite emission, in which the perovskite emission is the strongest peak. Even in optimized conditions, some effect

related to beam damage is persistently observed in the form of an intermediate broad peak at higher energies. TRCL of the polycrystalline film showed short lived charge carriers dynamics compared to photoluminescence, suggesting additional electron beam-specimen interactions to be further investigated. The optimization described in this work will help to unlock the use of CL hyperspectral mapping and TRCL on the more beam-sensitive hybrid perovskite compositions.

As SEM-CL systems with PM capabilities become prevalent and equipped with more sensitive and faster detectors, we anticipate that CL will play a large role in not only resolving the complex heterogeneity of the materials in the family of hybrid perovskites, but also in understanding the properties and degradation of many other novel beam sensitive semiconductors.

Acknowledgments

J F O and C D acknowledge funding from the Engineering and Physical Sciences Research Council (EPSRC) Nano Doctoral Training Centre (EP/L015978/1). J F O and S D S acknowledge the European Research Council (ERC) under the European Union's Horizon 2020 research and innovation programme (HYPERION, grant agreement no. 756962). E M T thanks the ERC Horizon 2020 research and innovation programme (Marie Skłodowska-Curie, grant agreement no. 841265). S D S and E M T acknowledge funding from the EPSRC (EP/R023980/1), from the EPSRC Centre for Advanced Materials for Integrated Energy Systems (CAM-IES, EP/P007767/1), and the Cambridge Royce facilities grant (EP/P024947/1). CL studies were supported by the EPSRC (EP/R025193/1). Dr Christian Monachon from Attolight is thanked for his ongoing support of the CL system. Yu-Hsien Chiang is thanked for his support in the sample preparation.

Data availability statement

The data that support the findings of this study are openly available at the following URL/DOI:https://doi.org/10.17863/CAM.62752.

Author contributions

J F O collected, analysed and interpreted all the CL maps. J F O and G K collected, analysed and interpreted the TRCL data. E M T and G K assisted in setting up the SEM for CL and in interpreting the CL maps. S M prepared samples and assisted in interpretation of the TRCL data. G D and C D supervised J F O. S D S supervised J.F.O, E. M.T and S.M and provided input on data interpretations. R A O supervised G K. J F O and E M T designed the work. All authors contributed to writing the manuscript.

ORCID iDs

Jordi Ferrer Orri https://orcid.org/0000-0002-0432-5932
Elizabeth M Tennyson https://orcid.org/0000-0003-0071-8445
Gunnar Kusch https://orcid.org/0000-0003-2743-1022
Giorgio Divitini https://orcid.org/0000-0003-2775-610X
Stuart Macpherson https://orcid.org/0000-0003-3758-1198
Samuel D Stranks https://orcid.org/0000-0002-8303-7292

References

[1] Snaith H J 2013 Perovskites: the emergence of a new Era for low-cost, high-efficiency solar cells *J. Phys. Chem. Lett.* **4** 3623–30
[2] Tennyson E M, Doherty T A S and Stranks S D 2019 Heterogeneity at multiple length scales in halide perovskite semiconductors *Nat. Rev. Mater.* 1–15
[3] Yacobi B G and Holt D B 2013 *Cathodoluminescence Microscopy of Inorganic Solids* (New York: Springer Science & Business Media)
[4] Guthrey H and Moseley J 2020 A review and perspective on cathodoluminescence analysis of halide perovskites *Adv. Energy Mater.* **10** 1903840
[5] Milosavljević A R, Huang W, Sadhu S and Ptasinska S 2016 Low-energy electron-induced transformations in organolead halide perovskite *Angew. Chem. Int. Ed.* **55** 10083–7
[6] Hentz O, Zhao Z and Gradečak S 2016 Impacts of ion segregation on local optical properties in mixed halide perovskite films *Nano Lett.* **16** 1485–90
[7] Tian Y, Peter M, Unger E, Abdellah M, Zheng K, Pullerits T, Yartsev A, Sundström V and Scheblykin I G 2015 Mechanistic insights into perovskite photoluminescence enhancement: light curing with oxygen can boost yield thousandfold *Phys. Chem. Chem. Phys.* **17** 24978–87

[8] Xiao C *et al* 2015 Mechanisms of electron-beam-induced damage in perovskite thin films revealed by cathodoluminescence spectroscopy *J. Phys. Chem. C* **119** 26904–11
[9] Li W *et al* 2017 Phase segregation enhanced ion movement in efficient inorganic CsPbIBr2 solar cells *Adv. Energy Mater.* **7** 1700946
[10] Lin Y-H *et al* 2020 A piperidinium salt stabilizes efficient metal-halide perovskite solar cells *Science* **369** 96–102
[11] Bischak C G, Hetherington C L, Wu H, Aloni S, Ogletree D F, Limmer D T and Ginsberg N S 2017 Origin of reversible photoinduced phase separation in hybrid perovskites *Nano Lett.* **17** 1028–33
[12] Merano M *et al* 2005 Probing carrier dynamics in nanostructures by picosecond cathodoluminescence *Nature* **438** 479–82
[13] Steckenborn A, Münzel H and Bimberg D 1981 Cathodoluminescence lifetime pattern of GaAs surfaces around dislocations *J. Lumin.* **24–25** 351–4
[14] Cortecchia D, Lew K C, So J-K, Bruno A and Soci C 2017 Cathodoluminescence of self-organized heterogeneous phases in multidimensional perovskite thin films *Chem. Mater.* **29** 10088–94
[15] Zhao B *et al* 2020 Efficient light-emitting diodes from mixed-dimensional perovskites on a fluoride interface *Nat. Electron.* **3** 704–10
[16] Merano M, Collin S, Renucci P, Gatri M, Sonderegger S, Crottini A, Ganière J D and Deveaud B 2005 High brightness picosecond electron gun *Rev. Sci. Instrum.* **76** 085108
[17] VandenBussche E J and Flannigan D J 2019 Reducing radiation damage in soft matter with femtosecond-timed single-electron packets *Nano Lett.* **19** 6687–94
[18] VandenBussche E J, Clark C P, Holmes R J and Flannigan D J 2020 Mitigating damage to hybrid perovskites using pulsed-beam TEM *ACS Omega* **5** 31867–71
[19] Saliba M *et al* 2016 Cesium-containing triple cation perovskite solar cells: improved stability, reproducibility and high efficiency *Energy Environ. Sci.* **9** 1989–97
[20] Bi D *et al* 2016 Efficient luminescent solar cells based on tailored mixed-cation perovskites *Sci. Adv.* **2** e1501170
[21] Ferrer Orri J, Lähnemann J, Prestat E, Johnstone D N and Tappy N 2021 *LumiSpy/lumispy: First release of Lumispy* (Zenodo)
[22] Wang Y, Sun Y-Y, Zhang S, Lu T-M and Shi J 2016 Band gap engineering of a soft inorganic compound PbI2 by incommensurate van der waals epitaxy *Appl. Phys. Lett.* **108** 013105
[23] Riesen N, Lockrey M, Badek K and Riesen H 2019 On the origins of the green luminescence in the 'zero-dimensional perovskite' Cs4PbBr6: conclusive results from cathodoluminescence imaging *Nanoscale* **11** 3925–32
[24] Kahmann S, Tekelenburg E K, Duim H, Kamminga M E and Loi M A 2020 Extrinsic nature of the broad photoluminescence in lead iodide-based ruddlesden–popper perovskites *Nat. Commun.* **11** 2344
[25] Lifshitz E, Bykov L, Yassen M and Chen-Esterlit Z 1997 The investigation of donor and acceptor states in nanoparticles of the layered semiconductor PbI2 *Chem. Phys. Lett.* **273** 381–8
[26] Azpiroz J M, Mosconi E, Bisquert J and Angelis F D 2015 Defect migration in methylammonium lead iodide and its role in perovskite solar cell operation *Energy Environ. Sci.* **8** 2118–27
[27] Yuan H *et al* 2016 Degradation of methylammonium lead iodide perovskite structures through light and electron beam driven ion migration *J. Phys. Chem. Lett.* **7** 561–6
[28] deQuilettes D W, Zhang W, Burlakov V M, Graham D J, Leijtens T, Osherov A, Bulović V, Snaith H J, Ginger D S and Stranks S D 2016 Photo-induced halide redistribution in organic–inorganic perovskite films *Nat. Commun.* **7** 11683
[29] Motti S G, Meggiolaro D, Martani S, Sorrentino R, Barker A J, Angelis F D and Petrozza A 2019 Defect activity in lead halide perovskites *Adv. Mater.* **31** 1901183
[30] Andaji-Garmaroudi Z *et al* 2020 Elucidating and mitigating degradation processes in perovskite light-emitting diodes *Adv. Energy Mater.* **10** 2002676
[31] Cacovich S, Messou D, Bercegol A, Béchu S, Yaiche A, Shafique H, Rousset J, Schulz P, Bouttemy M and Lombez L 2020 Light-induced passivation in triple cation mixed halide perovskites: interplay between transport properties and surface chemistry *ACS Appl. Mater. Interfaces* **12** 34784–94
[32] Tiede D O, Calvo M E, Galisteo-López J F and Míguez H 2020 Local rearrangement of the iodide defect structure determines the phase segregation effect in mixed-halide perovskites *J. Phys. Chem. Lett.* **11** 4911–6
[33] Hintermayr V A, Richter A F, Ehrat F, Döblinger M, Vanderlinden W, Sichert J A, Tong Y, Polavarapu L, Feldmann J and Urban A S 2016 Tuning the optical properties of perovskite nanoplatelets through composition and thickness by ligand-assisted exfoliation *Adv. Mater.* **28** 9478–85
[34] Wang Y, Lü X, Yang W, Wen T, Yang L, Ren X, Wang L, Lin Z and Zhao Y 2015 Pressure-induced phase transformation, reversible amorphization, and anomalous visible light response in organolead bromide perovskite *J. Am. Chem. Soc.* **137** 11144–9
[35] Diab H *et al* 2017 Impact of reabsorption on the emission spectra and recombination dynamics of hybrid perovskite single crystals *J. Phys. Chem. Lett.* **8** 2977–83
[36] Bischak C G, Sanehira E M, Precht J T, Luther J M and Ginsberg N S 2015 Heterogeneous charge carrier dynamics in organic–inorganic hybrid materials: nanoscale lateral and depth-dependent variation of recombination rates in methylammonium lead halide perovskite thin films *Nano Lett.* **15** 4799–807
[37] Besral N, Paul T, Thakur S, Sarkar S, Sardar K, Chanda K, Das A and Chattopadhyay K K 2018 Low dimensional $CH_3NH_3PbBr_3$ cubes for persistent luminescence: Energy variation of electron excitation *AIP Conf. Proc.* **1942** 120027
[38] Gelhausen O, Phillips M R and Toth M 2001 Depth-resolved cathodoluminescence microanalysis of near-edge emission in III-nitride thin films *J. Appl. Phys.* **89** 3535–7
[39] Rehman W, Milot R L, Eperon G E, Wehrenfennig C, Boland J L, Snaith H J, Johnston M B and Herz L M 2015 Charge-carrier dynamics and mobilities in formamidinium lead mixed-halide perovskites *Adv. Mater.* **27** 7938–44
[40] Herz L M 2016 Charge-carrier dynamics in organic-inorganic metal halide perovskites *Annu. Rev. Phys. Chem.* **67** 65–89
[41] Zhu T, Gachet D, Tang F, Fu W Y, Oehler F, Kappers M J, Dawson P, Humphreys C J and Oliver R A 2016 Local carrier recombination and associated dynamics in m-plane InGaN/GaN quantum wells probed by picosecond cathodoluminescence *Appl. Phys. Lett.* **109** 232103
[42] Klein-Kedem N, Cahen D and Hodes G 2016 Effects of light and electron beam irradiation on halide perovskites and their solar cells *Acc. Chem. Res.* **49** 347–54